Exotic and $q\bar{q}$ resonances in the $\pi^+\pi^-\pi^-$ system produced in π^-p collisions at 18 GeV/c

S. U. Chung, K. Danyo, R. W. Hackenburg, C. Olchanski,* J. S. Suh, and H. J. Willutzki
Department of Physics, Brookhaven National Laboratory, Upton, New York 11973

S. P. Denisov, V. Dorofeev, V. V. Lipaev, A. V. Popov, and D. I. Ryabchikov
Institute for High Energy Physics, Protvino, 142284 Russian Federation

Z. Bar-Yam, J. P. Dowd, P. Eugenio,† M. Hayek,‡ W. Kern, E. King, and N. Shenhav‡
Department of Physics, University of Massachusetts Dartmouth, North Dartmouth, Massachusetts 02747

V. A. Bodyagin, O. L. Kodolova, V. L. Korotkikh, M. A. Kostin, A. I. Ostrovidov,§ L. I. Sarycheva, I. N. Vardanyan, and A. A. Yershov
Nuclear Physics Institute, Moscow State University, Moscow, 119899 Russian Federation

D. S. Brown,‖ X. L. Fan, D. Joffe, T. K. Pedlar,¶ K. K. Seth, and A. Tomaradze
Department of Physics, Northwestern University, Evanston, Illinois 60208

T. Adams,† J. M. Bishop, N. M. Cason, E. I. Ivanov,** J. M. LoSecco, J. J. Manak, W. D. Shephard, D. L. Stienike, and S. A. Taegar
Department of Physics, University of Notre Dame, Notre Dame, Indiana 46556

G. S. Adams, J. P. Cummings, J. Hu,* J. Kuhn, M. Lu, J. Napolitano, D. B. White, and M. Witkowski
Department of Physics, Rensselaer Polytechnic Institute, Troy, New York 12180

M. Nozar, X. Shen,†† and D. P. Weygand
Thomas Jefferson National Accelerator Facility, Newport News, Virginia 23606

(E852 Collaboration)

(Received 19 November 2001; published 12 March 2002)

A partial-wave analysis of the reaction $\pi^-p\to\pi^+\pi^-\pi^-p$ at 18 GeV/c has been performed on a data sample of 250 000 events obtained in the Brookhaven experiment E852. The well-known $a_1(1260)$, $a_2(1320)$ and $\pi_2(1670)$ resonant states are observed. The existence of the $\pi(1800)$, $a_1(1700)$ and $a_4(2040)$ states is confirmed. The $a_3(1874)$ state is also observed. The exotic 1^{-+} $\pi_1(1600)$ state produced in the natural parity exchange process is found to decay in the $\rho(770)\pi^-$ channel. A mass-dependent fit results in a resonance mass of $1593\pm8^{+29}_{-47}$ MeV/c^2 and a width of $168\pm20^{+150}_{-12}$ MeV/c^2.

DOI: 10.1103/PhysRevD.65.072001 PACS number(s): 12.39.Mk, 13.25.Jx, 13.85.Hd, 14.40.Cs

I. INTRODUCTION

As a part of the experiment E852 at the Brookhaven National Laboratory, we have made a study of the reaction

$$\pi^-p\to\pi^+\pi^-\pi^-p. \tag{1}$$

In this paper we present the details of the analysis of which partial results were reported in our Letter [1]. The primary goal of this study was to search for the ''exotic'' mesons—states which lie outside the scope of the constituent quark model. Quantum chromodynamics predicts the existence of multiquark $q\bar{q}q\bar{q}$ and hybrid $q\bar{q}g$ mesons. Experimental identification of these non-$q\bar{q}$ mesons is difficult. For most of them, only some peculiar properties (unusual branching ratios, widths or production mechanisms [2]) may serve as indirect hints of their nature. However, some of these states should have $J^{PC}=0^{--},0^{+-},1^{-+},2^{+-},\ldots$ quantum numbers which are forbidden for simple $q\bar{q}$ mesons. In the reaction under study, the only allowed ''exotic'' quantum numbers for states with $J\leqslant2$ are $J^{PC}=1^{-+}$.

Several isovector 1^{-+} exotic candidates have been reported recently. A 1^{-+} signal in the $\eta\pi$ channel has been seen by several groups. Although early measurements [3,4]

*Present address: TRIUMF, Vancouver, Canada.
†Present address: Department of Physics, Florida State University, Tallahassee, FL 32306.
‡Permanent address: Rafael, Haifa, Israel.
§Also at Department of Physics, University of Notre Dame, Notre Dame, IN 46556.
‖Present address: Department of Physics, University of Maryland, College Park, MD 20742.
¶Present address: Laboratory for Nuclear Studies, Cornell University, Ithaca, NY 14853.
**Present address: Department of Physics, Idaho State University, Pocatello, ID 83209.
††Permanent address: Institute of High Energy Physics, Beijing, China.

were inconclusive, the most recent measurements [5,6] have presented strong evidence for a 1^{-+} state near 1.4 GeV/c^2. A possible 1^{-+} signal at a mass of 1.6 GeV/c^2 was observed in the $\eta'\pi$ [4,7,8], $\rho\pi$ [8,9] and $b_1\pi$ [8] channels. Additionally, a state with resonant phase behavior above 1.9 GeV/c^2 has been seen in the $f_1\pi$ [10] channel.

Theoretical predictions for the mass of the lightest 1^{-+} hybrid meson are based on various models. The flux tube model [11] predicts a 1^{-+} state at $1.8-2.0$ GeV/c^2. Similar results are obtained in the calculations based upon lattice QCD in the quenched approximation [12]. Earlier bag model estimates suggest somewhat lower masses in the $1.3-1.8$ GeV/c^2 range [13]. QCD sum-rule predictions vary widely between 1.5 GeV/c^2 and 2.5 GeV/c^2 [14]. The diquark cluster model [15] predicts the 1^{-+} state to be at 1.4 GeV/c^2, and the constituent gluon model [16] concludes that light exotics should lie in the region $1.8-2.2$ GeV/c^2. Most of these models (see Ref. [17]) predict a characteristic decay mode of the 1^{-+} hybrid into an $S+P$ meson combination such as $b_1(1235)\pi$ and $f_1(1285)\pi$. The probability of the $\rho\pi$ decay is expected to be significantly smaller. Typical partial widths for a 1^{-+} hybrid decay in the flux tube model are [18]

$$b_1\pi : f_1\pi : \rho\pi = 170 : 60 : 10 \ \text{MeV}/c^2. \tag{2}$$

The 3π final state was studied intensively during the past decades from the point of view of conventional mesons. However, recent developments in meson spectroscopy have raised interest in revisiting this reaction in search of exotic mesons.

II. EXPERIMENTAL APPARATUS

Experiment E852 was conducted at the Alternating Gradient Synchrotron (AGS) at the Brookhaven National Laboratory (BNL) with the Multi-Particle Spectrometer (MPS) augmented by additional detectors. A diagram of the experimental apparatus is shown in Fig. 1. A Cherenkov tagged π^- beam of momentum 18.3 GeV/c and a 30 cm liquid hydrogen target were used. The target was placed at the center of the MPS magnet with a field of 1 Tesla. The target was surrounded by a four-layer cylindrical drift chamber (TCYL) [19] used to trigger on the charged recoil particle, and a 198-element cylindrical thallium-doped cesium iodide array (CsI) [20] to reject events with soft photons. The downstream part of the magnet was equipped with 6 seven-plane drift chamber modules (DM1-6) [21] for charged-particle tracking. A large two-plane drift chamber (TDX4) was added to improve the momentum resolution. Triggering on the multiplicity of forward charged tracks was allowed by three proportional wire chambers (TPX1-3). Photon Hermiticity was ensured by a window-frame lead scintillator photon veto counter (DEA) in combination with an upstream segmented scintillator counter to identify charged tracks entering DEA. Non-interacting beam and elastic scattering events were rejected with the help of two forward scintillator counters (Beam Veto). Forward photons were detected by a 3000-element lead glass electromagnetic calorimeter (LGD) [22]. The trigger included a requirement on the total energy or invariant mass of all signals registered in the LGD. The data acquisition system typically accepted about 700 events per second. More details about the apparatus can be found in Ref. [23].

III. DATA SAMPLE

The trigger for reaction (1) was based on the requirement of three forward charged tracks and one charged recoil track. Seventeen million triggers of this type were recorded during the 1994 run of the experiment. The following criteria were used for the off-line event selection:

(i) There should be a fully reconstructed beam track, two negative (π^-) and one positive (π^+) downstream tracks and one charged recoil track (p) originating at a common vertex (only the direction of the recoil track was measured).

(ii) The vertex should be within the target volume.

(iii) No photons should be registered in DEA and LGD (the detector has almost 4π veto coverage for γ's).

(iv) The square of the missing mass calculated from the beam and downstream tracks should be less than 2.0 $(\text{GeV}/c^2)^2$.

(v) A SQUAW [24] kinematic 1-C fit to the recoil proton mass for the reaction $\pi^- p \to \pi^+\pi^-\pi^- p$ based on a full covariance matrix from track and vertex reconstruction is used. The recoil track direction is not taken into account in the kinematic fit. The confidence level of the fit is required to be at least 10%.

(vi) The direction of the missing momentum vector after the SQUAW fit is required to be within $\pm 20°$ in azimuth from the direction of the recoil track.

(vii) The energy deposit in the CsI detector surrounding the target should be $\leqslant 20$ MeV (beyond that associated with the recoil track) to reject events with soft π^o's from decays of recoil baryon isobars.

Approximately 700 000 events out of 17 million initial triggers satisfied the first three criteria as events with the correct track topology. The remaining criteria are kinematic cuts. They reduced this number to the final sample of 250 000 events used in the partial-wave analysis (PWA). Application of such strict cuts was justified by the goal of in-

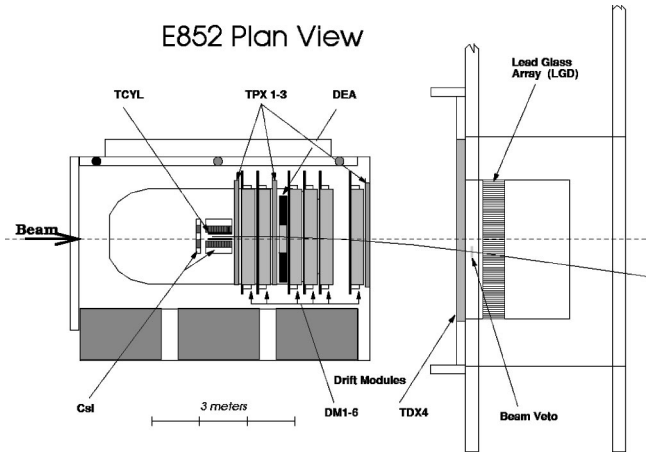

FIG. 1. Diagram of the experimental apparatus.

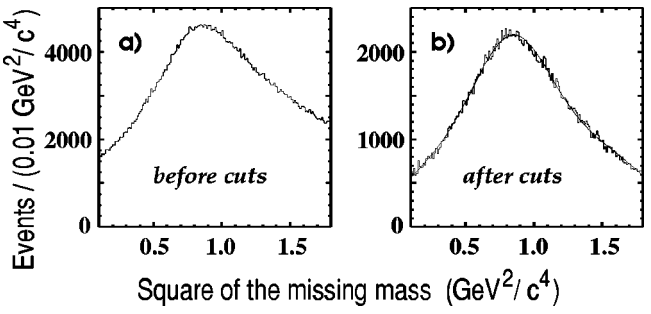

FIG. 2. Experimental distribution of the square of the missing mass: (a) Without cuts on soft π^o's and azimuthal angle between recoil track and missing momentum; (b) after the cuts. The curve represents a fit with a Gaussian function centered at the square of the proton mass with $\sigma=0.260$ $(\mathrm{GeV}/c^2)^2$.

suring that all events are exclusively proton recoil events. This is important in order to reduce the rank of the spin-density matrix to be fitted in the partial-wave analysis. Figure 2 shows the missing mass squared distribution without the cuts on soft π^o's and the difference in the azimuthal angle between the recoil and missing momenta [Fig. 2(a)] and after such cuts [Fig. 2(b)]. One can see that the distribution with cuts is perfectly Gaussian—centered at a recoil proton mass and has a width of 0.260 $(\mathrm{GeV}/c^2)^2$—while the uncut distribution has a large high mass tail from baryon isobars.

The missing mass plot in Fig. 2 demonstrates the absence of contamination by baryon recoil isobars from the background events of the $\pi^- p \to 3\pi\Delta \to 3\pi p$ (undetected pion) variety. However, it does not address such background reactions as $\pi^- p \to 2\pi\Delta \to 3\pi p$. The level of this contamination can be estimated from a plot of πp invariant mass (Fig. 3). There are no visible peaks from Δ's or N^*'s in this spectrum. We conclude that a contamination by baryon recoil isobars in the final data sample is insignificant.

Figure 4 shows acceptance-corrected $\pi^+\pi^-\pi^-$ [Fig. 4(a)] and $\pi^+\pi^-$ [Fig. 4(b)] mass spectra. The well-known resonances $a_1(1260)$, $a_2(1320)$ and $\pi_2(1670)$ are dominant. The two-body mass spectrum shows clear evidence of the $\rho(770)$ and $f_2(1270)$ isobars.

The shape of the full experimental acceptance is shown in Fig. 5 as a function of the $\pi^+\pi^-\pi^-$ [Fig. 5(a)] and $\pi^+\pi^-$

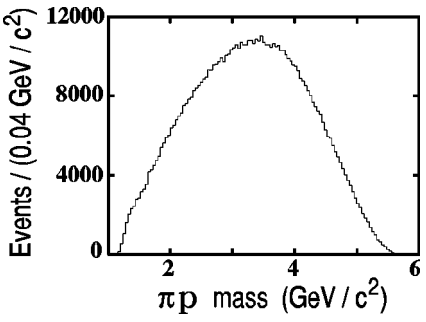

FIG. 3. Invariant mass distribution of the proton and one of the three pions (3 entries per event) for the final data sample. There is no visible recoil baryon contamination of the spectrum.

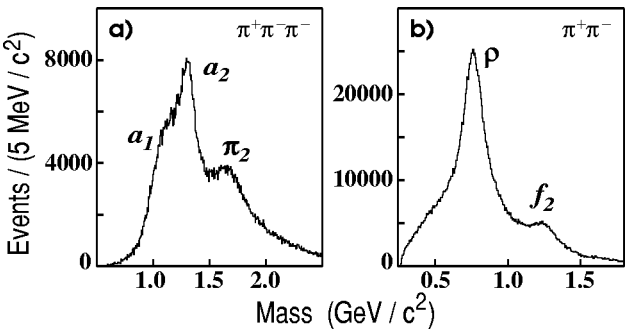

FIG. 4. Experimental invariant mass distribution with acceptance correction: (a) $\pi^+\pi^-\pi^-$ mass spectrum; (b) $\pi^+\pi^-$ mass spectrum (two entries per event).

[Fig. 5(b)] mass as well as a function of the polar angle $\cos\theta_{GJ}$ [Fig. 5(c)] and azimuthal angle ϕ_{TY} [Fig. 5(d)] in the Gottfried-Jackson frame. We wish to point out a sharp drop in the acceptance near $\cos\theta_{GJ}=+1$ (and a smaller drop near $\cos\theta_{GJ}=-1$). This fact will be used later in connection with possible ''leakage'' between waves in the partial-wave analysis. The average experimental acceptance is 24%. This number includes not only geometric acceptance but also estimated inefficiencies of the detectors and reconstruction program as well as effects of the data selection cuts. The acceptance is fairly flat as a function of momentum transfer t except for a sharp drop at $|t|<0.08$ $(\mathrm{GeV}/c)^2$. A fit to the corrected t distribution of the data with a form $e^{-b|t|}$ yields a value of the slope $b=6.0\pm0.1$ $(\mathrm{GeV}/c)^{-2}$.

IV. PARTIAL-WAVE ANALYSIS

The PWA analysis was performed using a program developed at BNL [25]. Each event is considered in the framework of the isobar model: a three-pion system and a recoil proton are produced in the initial collision of the incident π^- with the target proton. Then the three-pion system decays into a $\pi\pi$ isobar and an unpaired pion followed by the subsequent decay of the isobar. Each partial wave α is characterized by

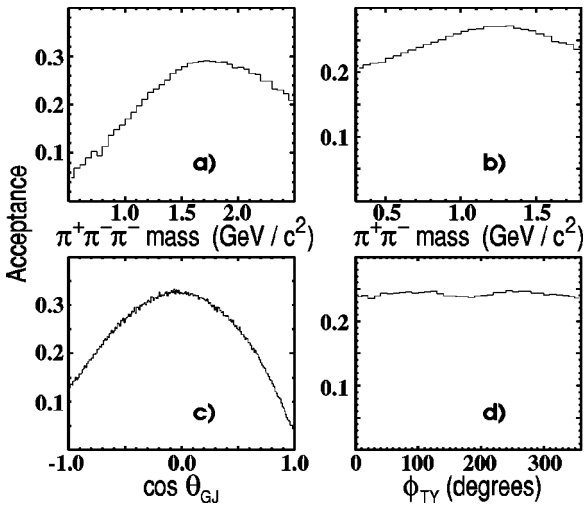

FIG. 5. Full experimental acceptance as a function of (a) $\pi^+\pi^-\pi^-$ mass; (b) $\pi^+\pi^-$ mass; (c) $\cos\theta_{GJ}$; (d) ϕ_{TY}.

the quantum numbers $J^{PC}[isobar]LM^{\epsilon}$—here J^{PC} are spin, parity and C parity of the partial wave; M is the absolute value of the spin projection on the quantization axis; ϵ is the reflectivity (and corresponds to the naturality of the exchanged particle); L is the orbital angular momentum between the isobar and the unpaired pion.

The spin-density matrix, $\rho^{\epsilon}_{\alpha\alpha'}$, is parametrized in terms of the complex production amplitudes $V^{k\epsilon}_{\alpha}$ for wave α with reflectivity ϵ [26]:

$$\rho^{\epsilon}_{\alpha\alpha'} = \sum_{k} V^{k\epsilon}_{\alpha} V^{k\epsilon}_{\alpha'} *. \tag{3}$$

These amplitudes are determined from an extended maximum likelihood fit (see Ref. [25]). The spin-density matrix is block-diagonal in reflectivity ϵ: waves with different reflectivity do not interfere. The index k corresponds to the different possibilities at the baryon vertex and defines the rank of the spin-density matrix. This rank does not exceed 2 for the proton-recoil reaction (from proton spin-non-flip and spin-flip contributions).

The experimental acceptance is taken into account by means of Monte Carlo normalization integrals as described in Ref. [25]. Relativistic Breit-Wigner functions with standard Blatt-Weisskopf barrier penetration factors and parameters from the Particle Data Group (PDG) [27] were used in the description of the $\rho(770)$, $f_2(1270)$, and $\rho_3(1690)$ isobars. The $\pi^+\pi^-$ S-wave parametrization is significantly more complex due to the presence of a few overlapping spin zero isobars and strong final state interactions involved. We have tried a number of different approaches. The simplest one was to describe the $f_o(980)$, σ and the ''glueball candidate'' $f_o(1500)$ [28] with Breit-Wigner forms. Other descriptions were based on a K-matrix approach [29]. We tried two model-dependent ways to use the K-matrix description. In one model (Q-vector) a $\pi\pi$ system is described by the elements of the matrix

$$T = (1 - iK\rho)^{-1} K \tag{4}$$

(ρ is the two-body phase space matrix), with $T_{11}(m)$ and $T_{21}(m)$ being the amplitudes for $\pi\pi \to \pi\pi$ and $KK \to \pi\pi$ re-scattering, respectively. In the other model (P-vector) the amplitude for a two-pion isobar β is described by the dynamic function

$$F_{\beta} = (1 - iK\rho)^{-1} P_{\beta}, \tag{5}$$

where P_{β} is the production vector of Aitchison [30]. In a very oversimplified picture, the $\pi\pi$ S-wave is separated into contributions from different channels in the Q-vector approach and from different isobars in the P-vector approach. Both cases converge to a standard Breit-Wigner description in the ''one isobar, one channel'' limit.

Different parametrizations of the K-matrix are available. We tried the Crystal Barrel parametrization with three K-matrix poles [28] as well as the ''K_1'' and ''M'' solutions of Au, Morgan, and Pennington (AMP) [31]. We came to the conclusion that most of our results are not very sensitive to the particular choice of the $\pi\pi$ isoscalar parametrization with the exception of the $J^{PC} = 0^{-+}$ waves as discussed later. Our final choice was to use the parametrization first suggested by VES [32]. In this parametrization, the $f_o(980)$ isobar is introduced as a pure Breit-Wigner state with an amplitude $\Delta^{f_o(980)}_{BW}(m)$, and the broad σ [or $f_o(400-1200)$] state has an amplitude

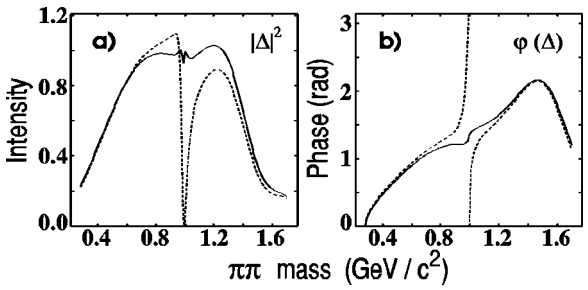

FIG. 6. Square of the $\pi\pi$ S-wave amplitude (a) and its phase (b) before (dashed line) and after (solid line) the subtraction of the $f_o(980)$ Breit-Wigner amplitude. See text for details.

$$\Delta^{\sigma}(m) = T_{11}(m) - c\,\Delta^{f_o(980)}_{BW}(m), \tag{6}$$

where $T_{11}(m)$ is taken from the ''M'' solution of AMP [31], and the complex constant c is fixed at the fitted value of $(-0.3743; 0.3197)$. The behavior of the square of the amplitude and phase of $\Delta^{\sigma}(m)$ [with and without the $f_o(980)$ ''subtraction''] is shown in Fig. 6. Such parametrization more closely follows the philosophy of the isobar model. Unless otherwise noted, all plots presented below were done for the PWA fits with this type of the parametrization.

Other conclusions from the study of the $\pi\pi$ S-wave parametrization in this reaction are (i) the contribution of the $KK \to \pi\pi$ channel in the Q-vector approach [i.e., the contribution of the $T_{21}(m)$ amplitude] is negligible, and (ii) the contribution of the $f_o(1500)$ in the P-vector approach is negligible.

The partial-wave analysis was performed in 40 MeV/c^2 mass bins (all plots of partial waves are shown with this bin size) and for $0.05 < -t < 1.0$ $(\mathrm{GeV}/c)^2$. Our selection of partial waves for the final fits was based on a philosophy of obtaining a good fit with a minimal number of the fitted parameters. This was achieved by determining a minimal set of partial waves which gave an adequate description of the observed angular distributions. Goodness of fit was estimated by a qualitative comparison of the experimental moments $H(LMN)$ with those predicted by the PWA fit [26]. These moments are the integrals of the $D^{L}_{MN}(\alpha,\beta,\gamma)$ functions taken over the experimental or predicted angular distributions $I(\alpha,\beta,\gamma)$:

$$H(LMN) = \int I(\alpha,\beta,\gamma) D^{L}_{MN}(\alpha,\beta,\gamma)\, d\alpha\, d\beta\, d\gamma. \tag{7}$$

Here α,β,γ are three Euler angles describing the orientation of a three-body system. In case of a 100% acceptance, index L can take values from 0 to twice the highest value of total spin J among all partial waves while indices M and N are limited by twice the highest value of the spin projection M

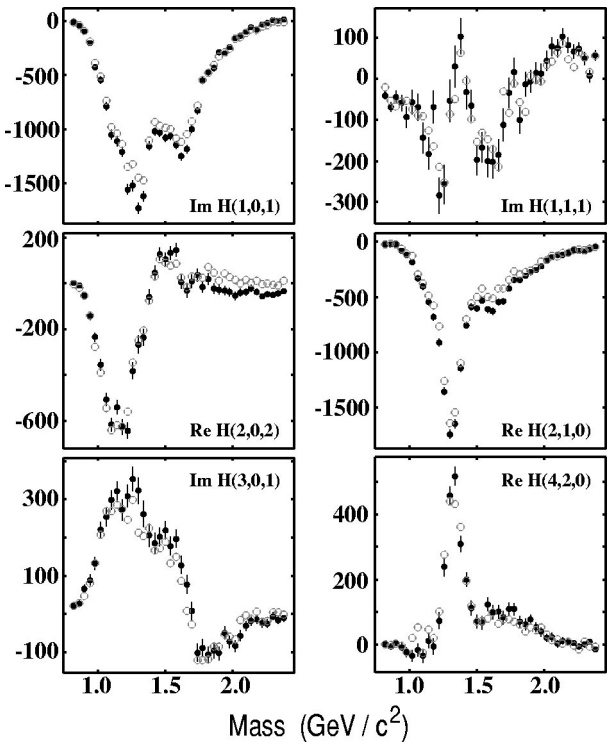

FIG. 7. Example of the comparison of the experimental (solid points with the error bars) and predicted (open circles) $H(LMN)$ moments in the 21-wave rank-1 fit.

among all partial waves. We found that a minimal set of 21 waves is needed to achieve an adequate description of the data below 1.8 GeV/c^2. The actual number of waves in the final fits was a function of the three-pion mass, starting with 14 waves below 1.4 GeV/c^2 and reaching 21 waves above 1.7 GeV/c^2. Figure 7 shows an example of comparison of the experimental and predicted moments in the fit with 21 waves for just a few largest moments (out of 59 non-zero moments for this set of waves). The 1^{-+} waves were found to be essential for the good description of the moments. The waves in the minimal set of waves (''21-wave fit'') are shown in Table I. This fit was used in Ref. [1] and its results are shown in this paper unless otherwise specified.

Results of an additional fit with 27 partial waves (''27-wave fit'') are also shown in this paper. The purpose of this fit was (a) to study the high-mass region where the 3^{++} and 4^{++} waves become important, and (b) to add small waves with structures at lower mass associated with the known states which were omitted from the 21-wave fit because they were not seen in the $H(LMN)$ moments. Many fits with different sets of waves (up to 70 waves) have been tried to determine the systematic errors in the results.

A flat background wave was included in all fits. This wave has an isotropic distribution and does not interfere with other waves. It absorbs both the physical background from the events of misidentified topologies and any contribution from the partial waves omitted in the fit. Thus, this wave can indirectly indicate both the quality of the data sample and the quality of the PWA model used. The magnitude of the background wave is compared with the total intensity in Fig. 8.

TABLE I. Partial waves used in the 21-wave fit of the 3π system and additional waves used in the 27-wave fit.

Partial waves in the 21-wave fit	
$J^{PC}=0^{-+}$:	$[f_o(980)]S0^+;[\sigma]S0^+;[\rho]P0^+$
$J^{PC}=1^{-+}$:	$[\rho]P0^-,P1^-,P1^+$
$J^{PC}=1^{++}$:	$[\rho]S1^-,S0^+,S1^+,D0^+$
$J^{PC}=2^{-+}$:	$[\sigma]D0^+;[\rho]P0^+;[f_2]S1^-,S0^+,S1^+,D0^+,D1^+$
$J^{PC}=2^{++}$:	$[\rho]D0^-,D1^+$
$J^{PC}=3^{++}$:	$[\rho_3]S0^+$
Background	
Additional partial waves in the 27-wave fit	
$J^{PC}=1^{++}$:	$[\sigma]P0^+$
$J^{PC}=2^{-+}$:	$[\rho]F0^+$
$J^{PC}=3^{++}$:	$[\rho]D0^+;[f_2]P0^+$
$J^{PC}=4^{++}$:	$[\rho]G1^+;[f_2]F1^+$

This wave is less than a few percent of the total number of events below 1.8 GeV/c^2 even in the simplest PWA model (21-wave rank-1 fit) which indicates that the spin-density matrix of this reaction has predominantly rank 1.

A. Results for non-exotic partial waves

The summary plot of the total intensities of the major J^{PC} waves is presented in Fig. 9. Decomposition of these waves is discussed below. Unless otherwise stated, the 21-wave rank-1 fit is shown in the plots. At the same time, the values of resonance parameters quoted in this section are based on multiple PWA fits with varying rank of fit, set of partial waves, etc. The quoted values for masses, widths, and branching ratios are calculated as the average over these multiple fits. The systematic errors reflect the spread of the obtained fitted parameters, while the statistical errors are the largest ones observed in these fits.

The mathematical form of the Breit-Wigner amplitudes used in the mass-dependent fits is given in Sec. V of Ref. [33]. Particle yields used in the branching ratios calculations were obtained by integrating the fitted Breit-Wigner curves.

$J^{PC}=2^{-+}$ *waves*

The most significant waves of this type are shown in Fig. 10. The $\pi_2(1670)$ resonance is seen in three decay channels:

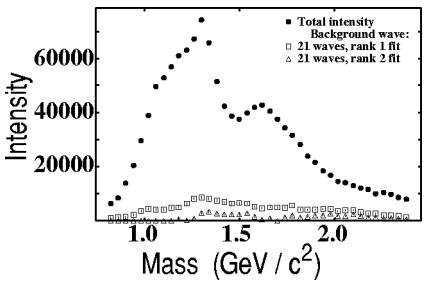

FIG. 8. Magnitude of the background wave for 2 different PWA fits—21-wave rank-1 fit (squares), 21-wave rank-2 fit (triangles)—with respect to the total intensity (solid circles).

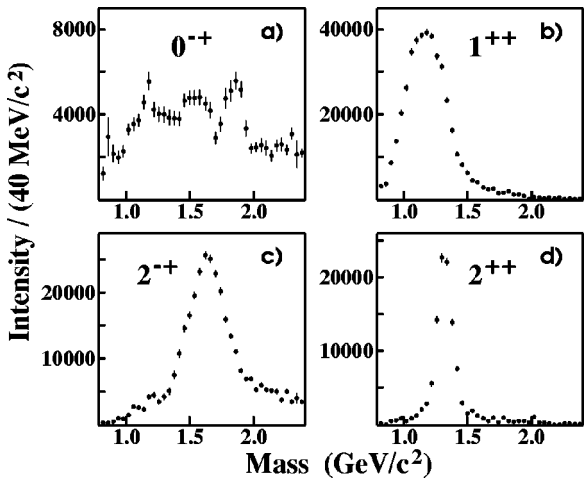

FIG. 9. Combined intensities of all (a) 0^{-+} waves, (b) 1^{++} waves, (c) 2^{-+} waves, (d) 2^{++} waves.

$f_2\pi$, $\rho\pi$ and $\sigma\pi$. The largest $\pi_2(1670)$ wave is $2^{-+}[f_2]S0^+$ [Fig. 10(a)]. Also shown is the $M^\epsilon=1^+$ wave which is at 10% level of the $M^\epsilon=0^+$ wave. A mass-dependent fit of this wave's intensity with a Breit-Wigner shape results in the following $\pi_2(1670)$ parameters:

$$M=1676\pm3\pm8\ \ \mathrm{MeV}/c^2,$$
$$\Gamma=254\pm3\pm31\ \ \mathrm{MeV}/c^2. \tag{8}$$

Here and below the first error values are statistical. They are based on the full error matrix obtained in the PWA likelihood fits. The second error values represent the systematic uncertainties. Presently, PDG [27] lists the following $\pi_2(1670)$ parameters: $M=1670\pm20$ MeV/c^2 and $\Gamma=259\pm11$ MeV/c^2. We show this wave first because of its well-established resonance nature. This makes it a natural choice for a reference wave in many phase analyses presented later in this paper.

The $2^{-+}[f_2]D0^+$ wave [Fig. 10(b)] differs in shape from the corresponding S wave: it appears to be wider and at higher mass than $\pi_2(1670)$. Such behavior was observed in the previous analyses of this reaction [32]. The rising phase of the D wave at 1.8 GeV/c^2 relative to the S wave [Fig. 11(a)] might be suggestive of an additional 2^{-+} state different from the $\pi_2(1670)$ (such a state is expected in the ^3P_o model [34]). However, other interpretations [for example, the interference of the $\pi_2(1670)$ state with its radial excitation above 2 GeV/c^2] are also possible.

The $2^{-+}[\sigma]D0^+$ wave [Fig. 10(c)] shows 2 structures on top of the monotonically rising background. The first peak is the $\pi_2(1670)$ state decaying through the $\pi\pi$ S-wave. The estimated ratio of the branching ratios is

$$\frac{BR[\pi_2(1670)\to f_2\pi, f_2\to\pi\pi]}{BR[\pi_2(1670)\to\sigma\pi,\sigma\to\pi\pi]}=4.9\pm0.6\pm2.0. \tag{9}$$

The large systematic error comes mostly from the uncertainty in the subtraction of the $\sigma\pi$ background underneath the $\pi_2(1670)$ as well as from the instability of its magnitude in different fits. The second structure in the $2^{-+}[\sigma]D0^+$ wave appears above 2 GeV/c^2. The same structure seems to be present in the $2^{-+}[\rho]F0^+$ wave [Fig. 10(e)] and, at a much lower level, in the $2^{-+}[\rho]P0^+$ wave [Fig. 10(d)]. The phase difference between the $2^{-+}[\sigma]D0^+$ and $0^{-+}[f_o(980)]S0^+$ waves is shown in Fig. 11(b). There is a clear phase motion due to the $\pi_2(1670)$ and $\pi(1800)$ states at 1.6 GeV/c^2 and 1.8 GeV/c^2, respectively. However, the interesting feature of this plot is an apparent rise in the 2^{-+} phase above 2 GeV/c^2 pointing to a possible $\pi_2(2100)$ state [27]—the first radial excitation of the $\pi_2(1670)$ [2].

In the $\rho\pi$ channel, the $\pi_2(1670)$ is seen both in the P and F waves. While a peak in the F wave [Fig. 10(e)] is quite clean, the structure in the P wave [Fig. 10(d)] is significantly wider than expected for the $\pi_2(1670)$ alone. Our studies lead us to believe that the $2^{-+}[\rho]P0^+$ spectrum is significantly distorted below 1.5 GeV/c^2 by "leakage" from the strong $1^{++}[\rho]S0^+$ wave. However, we believe that above 1.5 GeV/c^2 the intensity is essentially all due to the $\pi_2(1670)$, and the F/P ratio [Fig. 10(f)] is consistent with being constant. With this assumption, we obtain the following ratio of wave amplitudes:

$$\frac{F[\pi_2(1670)\to\rho\pi]}{P[\pi_2(1670)\to\rho\pi]}=-0.72\pm0.07\pm0.14. \tag{10}$$

With the same assumption for the $\rho\pi$ P wave, its total yield was obtained as the integral of a Breit-Wigner function of fixed mass and width, normalized to the slope of the $2^{-+}[\rho]P0^+$ intensity in the mass region above 1.6 GeV/c^2. The yields in the P and F waves as well as in the $M^\epsilon=0^+$ and $M^\epsilon=1^+$ were combined. The following ratio was obtained:

$$\frac{BR[\pi_2(1670)\to f_2\pi]}{BR[\pi_2(1670)\to\rho\pi]}=2.33\pm0.21\pm0.31. \tag{11}$$

The same ratio from the PDG [27] is 1.81 ± 0.3.

$J^{PC}=0^{-+}$ waves and $\pi(1800)$

The major 0^{-+} waves are shown in Fig. 12. The $0^{-+}[\rho]P0^+$ wave [Fig. 12(a)] reveals a broad $\pi(1300)$ resonance. The phase difference [Fig. 12(b)] between this wave and the $2^{-+}[f_2]S0^+$ wave [the strongest $\pi_2(1670)$ wave] confirms the resonant nature of the $\pi(1300)$: the phase difference is rising below 1.5 GeV/c^2 due to the rising Breit-Wigner phase motion of the $\pi(1300)$ and falling above that mass due to the rising phase of the $\pi_2(1670)$ state. This wave remains relatively stable regardless of the PWA model. The intensity of this wave was fitted with a Breit-Wigner shape on top of a linear-rising background resulting in the following parameters of the $\pi(1300)$ meson:

$$M=1343\pm15\pm24\ \ \mathrm{MeV}/c^2,$$
$$\Gamma=449\pm39\pm47\ \ \mathrm{MeV}/c^2. \tag{12}$$

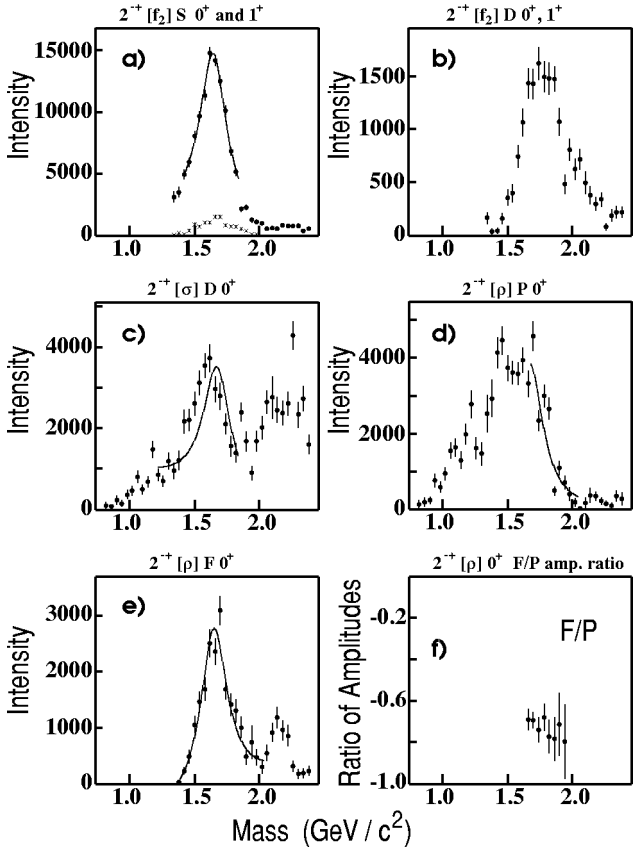

FIG. 10. (a) Intensity of the $2^{-+}[f_2]S0^+$ (points) and $2^{-+}[f_2]S1^+$ (crosses) waves; (b) combined intensity of the $2^{-+}[f_2]D\ M^{\epsilon}=0^+,1^+$ waves; (c) intensity of the $2^{-+}[\sigma]D0^+$ wave; (d) intensity of the $2^{-+}[\rho]P0^+$ wave; (e) intensity of the $2^{-+}[\rho]F0^+$ wave (27-wave fit); (f) ratio of the $2^{-+}[\rho]F0^+$ wave amplitude to the $2^{-+}[\rho]P0^+$ wave amplitude (27-wave fit). Curves show the mass-dependent fits of the $\pi_2(1670)$ with parameters from Eq. (8).

PDG [27] quotes the mass of this state as 1300 ± 100 MeV/c^2 with width from 200 MeV/c^2 to 600 MeV/c^2.

Intensities of the $0^{-+}[\sigma]S0^+$ and $0^{-+}[f_o(980)]S0^+$ waves are shown in Figs. 12(c,e) while their phase differences with respect to the same $2^{-+}[f_2]S0^+$ anchor wave are shown in Figs. 12(d,f). In earlier studies, we found no indication of the $\pi(1300)$ state in either the $f_o(980)\pi$ intensity or its phase. As a result, this wave was not used at low mass in the final fits. However, the $\sigma\pi$ channel shows a large intensity in the low mass region and a rising phase below 1.5 GeV/c^2 similar to the $\rho\pi$ channel. This indicates that the $\pi(1300)$ meson may decay to $\sigma\pi$. Unfortunately, the shape of the $\sigma\pi$ intensity at low mass is very complex and very unstable under different assumptions used in the PWA. This is illustrated in Fig. 13 where the intensity of the $0^{-+}S0^+$ waves (summed over all $\pi\pi$ S-wave isobars) is shown for 3 different fits: (a) 21-wave fit with the $\pi\pi$ *S*-wave parametrization from the "*M*" solution of Ref. [31] modified as described earlier; (b) 27-wave fit with the same parametrization; (c) 24-wave fit with a simple Breit-Wigner parametrization with parameters from the PDG [27]. Additional waves in the last fit are those involving the $f_o(1500)$ isobar. Variations in the shape of the low-mass end of the 0^{-+} intensity spectrum are obvious. Such instability under different PWA assumptions is not the only problem affecting the low-mass region of the $0^{-+}[\sigma]S0^+$ wave. A large nonresonant Deck-type background contribution is also expected in this wave [32] making the interpretation of the $\pi(1300)\rightarrow\sigma\pi$ decay channel even more difficult. In this analysis, no attempts were made to parametrize the Deck-type back-

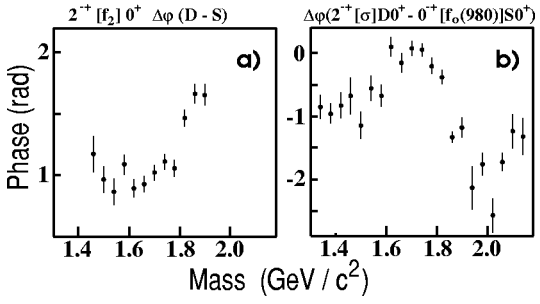

FIG. 11. Phase difference between (a) the $2^{-+}[f_2]D0^+$ and $2^{-+}[f_2]S0^+$ waves; (b) the $2^{-+}[\sigma]D0^+$ and $0^{-+}[f_o(980)]S0^+$ waves.

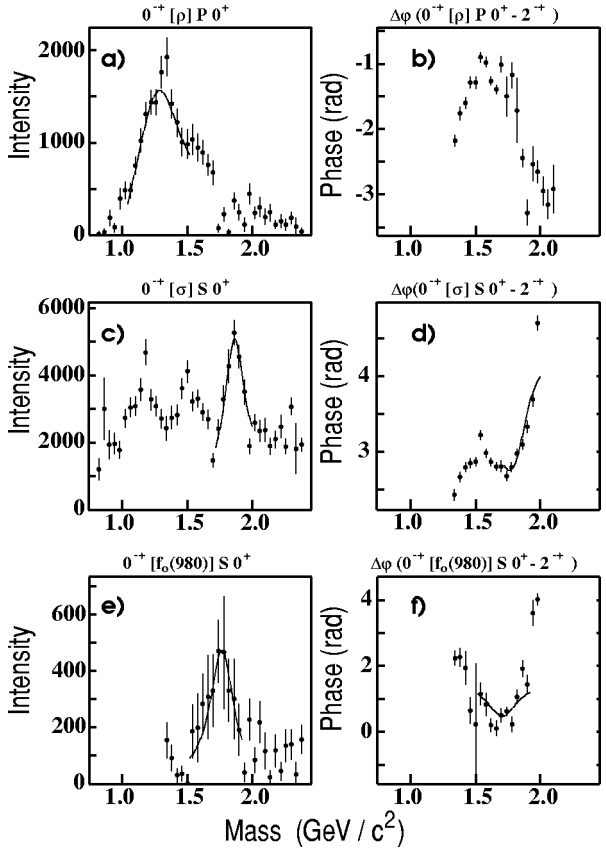

FIG. 12. Intensities of the (a) $0^{-+}[\rho]P0^+$, (c) $0^{-+}[\sigma]S0^+$, (e) $0^{-+}[f_o(980)]S0^+$ waves and their corresponding phase differences (b,d,f) with respect to the $2^{-+}[f_2]S0^+$ wave. Curves show the mass-dependent fits of (a) the $\pi(1300)$ with parameters from Eq. (12); (c,d) the $\pi(1800)$ with parameters from Eq. (14); (e,f) the $\pi(1800)$ with parameters from Eq. (13).

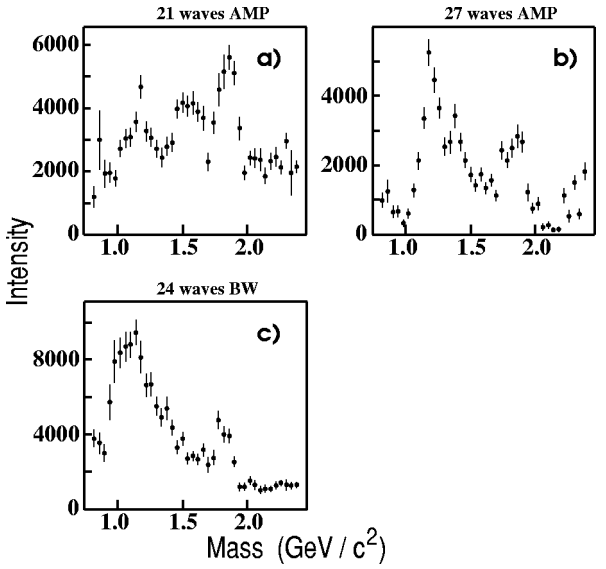

FIG. 13. Intensity of the $0^{-+}S0^{+}$ waves summed over $\pi\pi$ *S*-wave isobars for the different $\pi\pi$ *S*-wave parametrizations: (a) 21-wave fit, modified "*M*" solution parametrization; (b) 27-wave fit, same parametrization; (c) 24-wave fit, simple Breit-Wigner parametrization. See text for details.

ground. This does not affect the PWA results in any way but prevents us from doing mass-dependent fits of the PWA results where expected contribution of this background may be relatively important—namely, in the low-mass regions of the $0^{-+}[\sigma]$ and $1^{++}[\rho]$ waves.

Another feature of the 0^{-+} $\sigma\pi$ and $f_o(980)\pi$ waves is a clearly visible $\pi(1800)$ state [see Figs. 12(c,e)]. The corresponding phase differences [Figs. 12(d,f)] have an unambiguous resonant signature in the rapidly rising phase at 1.8 GeV/c^2. This resonance was seen first in Ref. [35] and studied in detail in Ref. [32]. We find the following $\pi(1800)$ parameters in the $f_o(980)\pi$ channel:

$$M = 1774 \pm 18 \pm 20 \ \text{MeV}/c^2,$$
$$\Gamma = 223 \pm 48 \pm 50 \ \text{MeV}/c^2. \tag{13}$$

These values are consistent with the results of the VES group obtained in the 3π channel [32]. They find the $\pi(1800)$ mass and width to be $1775 \pm 7 \pm 10$ MeV/c^2 and $190 \pm 15 \pm 15$ MeV/c^2, respectively. However, the $\pi(1800)$ appears to be shifted in the $\sigma\pi$ channel:

$$M = 1863 \pm 9 \pm 10 \ \text{MeV}/c^2,$$
$$\Gamma = 191 \pm 21 \pm 20 \ \text{MeV}/c^2. \tag{14}$$

The reason for this apparent shift is unclear. Note that measurements of the $\pi(1800)$ mass in some other channels also show a spread of about 100 MeV/c^2 [27]. This can be an artifact of the $\pi\pi$ *S*-wave parametrization or the result of the interference of the $\pi(1800)$ meson with the broad underlying $\pi(1300)$. The possibility that there are actually two different 0^{-+} states at this mass also cannot be excluded because both the 0^{-+} non-exotic hybrid meson and the second radial excitation of the pion are predicted to be at around this mass in the flux-tube model [36,34]. Under the assumption of a single state, the ratio of the $\pi(1800)$ decay into these 2 channels is

$$\frac{BR[\pi(1800) \to f_o(980)\pi, f_o \to \pi\pi]}{BR[\pi(1800) \to \sigma\pi, \sigma \to \pi\pi]} = 0.44 \pm 0.08 \pm 0.38. \tag{15}$$

This ratio is significantly smaller than the value of 1.7 ± 0.3 quoted in Ref. [32].

The $\pi(1800)$ state is hardly seen in the intensity or phase of the $\rho\pi$ wave [Figs. 12(a,b)]. We estimate that the $\rho\pi$ partial width is less than 25% of the $f_o(980)\pi$ partial width.

In view of a possible hybrid nature of the $\pi(1800)$, its possible decay through the gluon-rich $f_o(1500)$ state and a pion was also examined. We tried both *K*-matrix and Breit-Wigner parametrizations of the $f_o(1500)$ and came to the conclusion that the $\pi(1800) \to f_o(1500)\pi$ decay is not seen in this channel. This might be caused by the small branching ratio of the $f_o(1500)$ state into $\pi^+\pi^-$ [37].

$J^{PC}=1^{++}$ waves and $a_1(1700)$

The most dominant wave in reaction (1) is $1^{++}[\rho]S0^{+}$ [Fig. 14(a)]. It accounts for almost half of the total number of events. It has a broad structure at 1.2 GeV/c^2 with a width of 300 MeV/c^2 associated with the $a_1(1260)$ resonance. The phase of the $1^{++}[\rho]S0^{+}$ wave when compared with phases of other well-established states like the $a_2(1320)$ varies very slowly over the width of the $a_1(1260)$ state in accordance with the expectations of the Deck model [38]. The same state is seen in the $M^{\epsilon}=1^{+}$ projection wave [Fig. 14(a)] at the level of about 6% of the $M^{\epsilon}=0^{+}$ wave. The decay of the $a_1(1260)$ resonance through the σ ($\pi\pi$ *S*-wave) is also present in our data [Fig. 14(b)]. We do not fit the $a_1(1260)$ because contribution of the non-resonant Deck-type background into the 1^{++} signal at 1.2 GeV/c^2 may be significant [32], and subtraction of this background is not trivial.

The $1^{++}[\rho]D0^{+}$ wave in the 21-wave fit has a structure shown in Fig. 14(c). The first peak can be associated with the $a_1(1260)$. The phase difference between the $1^{++}[\rho]0^{+}$ *S* and *D* waves [Fig. 14(d)] is flat at the value of about 2.5 radians in the region of the $a_1(1260)$ state. The deviation of the phase difference from the exact value of π radians (as expected for a pure resonance with the same production but different decay amplitudes) can be explained by a small contribution of a non-resonant background. Above the $a_1(1260)$ region, the phase difference starts to fall rapidly, pointing to a resonant nature for the second peak in the *D* wave. A similar 1^{++} object was observed in Ref. [32]. It is usually interpreted as the first radial excitation of the $a_1(1260)$ resonance [34]. We obtain the following mass and width for the 1^{++} $a_1(1700)$ state:

$$M = 1714 \pm 9 \pm 36 \ \text{MeV}/c^2,$$
$$\Gamma = 308 \pm 37 \pm 62 \ \text{MeV}/c^2. \tag{16}$$

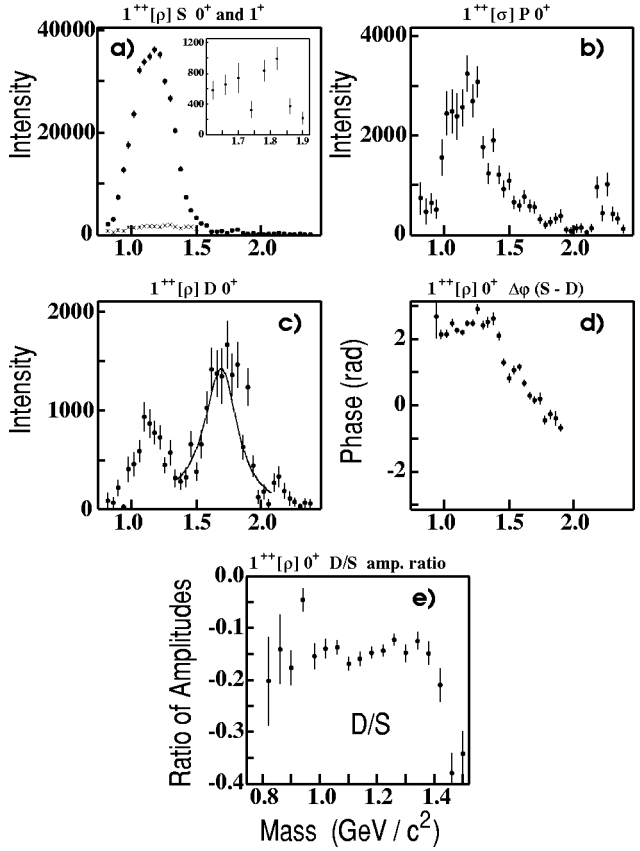

FIG. 14. (a) Intensity of the $1^{++}[\rho]S0^+$ (points) and $1^{++}[\rho]S1^+$ (crosses) waves. Inset shows the $M^\epsilon=0^+$ wave intensity in the $a_1(1700)$ region; (b) intensity of the $1^{++}[\sigma]P0^+$ wave (27-wave fit); (c) intensity of the $1^{++}[\rho]D0^+$ wave. Curve shows the mass-dependent fit of the $a_1(1700)$ with parameters from Eq. (16); (d) phase difference between the $1^{++}[\rho]S0^+$ and $1^{++}[\rho]D0^+$ waves; (e) ratio of the $1^{++}[\rho]D0^+$ wave amplitude to the $1^{++}[\rho]S0^+$ wave amplitude.

It is not clear if the $a_1(1700)$ state is also present in the S wave. While the $1^{++}[\rho]S0^+$ wave may have a shoulder in the intensity at 1.7 GeV/c^2 (at 50% level comparing to the D wave), no resonant phase motion is seen in the phase of the S wave at this mass.

The ratio of the D and S wave amplitudes for the decay $a_1(1260)\to\rho\pi$ is an important benchmark in many quark model calculations. The ^3P_o model [34] predicts this ratio to be $D/S=-0.15$. Our measured D/S ratio is shown in Fig. 14(e) for the case of the 21-wave fit. Note that we do not separate the $a_1(1260)$ state from the Deck-type background in this calculation. The ratio is fairly flat in the region of the $a_1(1260)$ with the mean value of

$$\frac{D[a_1(1260)\to\rho\pi]}{S[a_1(1260)\to\rho\pi]}=-0.14\pm0.04\pm0.07. \qquad (17)$$

The large systematic error is caused by the fact that the $1^{++}[\rho]D0^+$ wave becomes very unstable in the PWA fits if many additional waves are included. This instability also affects the appearance of the $a_1(1700)$ state: its intensity is greatly reduced in the PWA fits with larger numbers of partial waves while its resonant phase motion remains relatively stable.

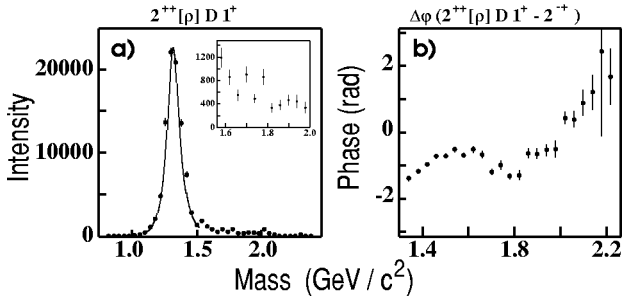

FIG. 15. (a) Intensity of the $2^{++}[\rho]D1^+$ wave with a high-mass region shown in the inset. The mass-dependent fit of the $a_2(1320)$ with parameters from Eq. (18) is also shown; (b) phase difference between the $2^{++}[\rho]D1^+$ and $2^{-+}[f_2]S0^+$ waves.

$J^{PC}=2^{++}$ wave

The strongest $M=1$ projection wave is $2^{++}[\rho]D1^+$ [Fig. 15(a)] showing the $a_2(1320)$ resonance. Parameters of the $a_2(1320)$ in our fit of the intensity peak are

$$M=1326\pm2\pm2 \ \text{MeV}/c^2,$$
$$\Gamma=108\pm3\pm15 \ \text{MeV}/c^2. \qquad (18)$$

The experimental resolution of 8 MeV/c^2 was unfolded. PDG values of the a_2 mass and width are $M=1317.9\pm1.3$ MeV/c^2 and $\Gamma=104.7\pm1.9$ MeV/c^2 [27]. The wave intensity at $1.7-1.8$ GeV/c^2 [where the $a_2(1700)$ state is expected in the quark model [2]] is at the level of about 3% of the $a_2(1320)$ peak. While the phase difference of the 2^{++} wave relative to the $2^{-+}[f_2]S0^+$ wave [Fig. 15(b)] exhibits a stable resonance-like rise above 1.8 GeV/c^2, no significant structure in the intensity is seen at this mass. Apparently, the $a_2(1700)$ state (if it exists) has a very small cross section or $\rho\pi$ branching ratio.

$J^{PC}=3^{++}$ waves and $a_3(1874)$

The $3^{++}M^\epsilon=0^+$ waves in the 27-wave fit are shown in Fig. 16: the $\rho\pi$ D wave [Fig. 16(a)], the $f_2\pi$ P wave [Fig. 16(c)], and the $\rho_3\pi$ S wave [Fig. 16(e)]. All waves exhibit a structure in the intensity and a tendency for a rising phase difference above 1.8 GeV/c^2 [Figs. 16(b,c,d)]. This indicates the presence of an a_3 state with

$$M=1874\pm43\pm96 \ \text{MeV}/c^2,$$
$$\Gamma=385\pm121\pm114 \ \text{MeV}/c^2. \qquad (19)$$

The VES group finds the same resonance with $M=1.86\pm0.02$ GeV/c^2 and $\Gamma=0.48\pm0.06$ GeV/c^2 [8]. This state lies lower than the 2.05 GeV/c^2 mass predicted in the quark model of Godfrey and Isgur [2]. The apparent distortion of the $a_3(1874)$ shape and phase in the $\rho_3(1690)\pi$ channel is due to the close proximity of the kinematic threshold: both

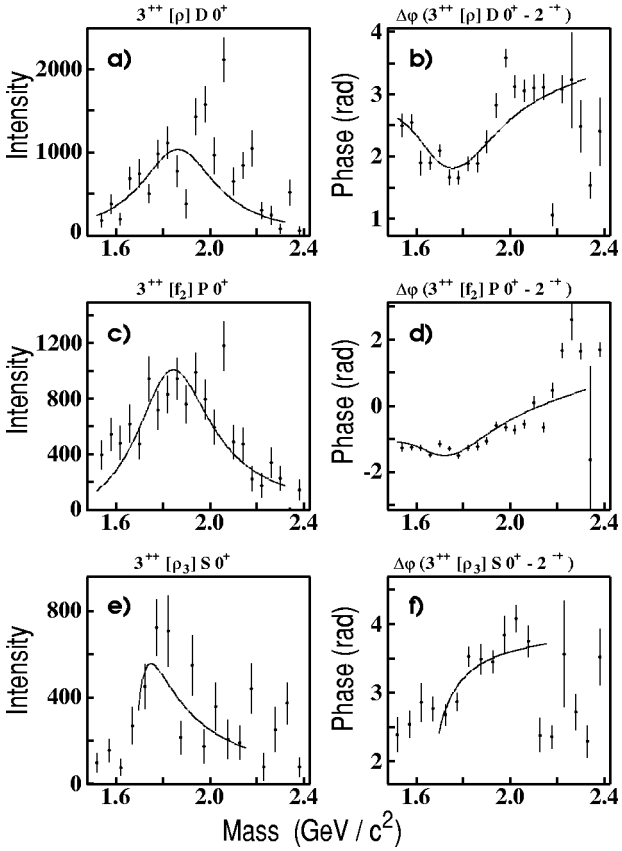

FIG. 16. Intensities of the (a) $3^{++}[\rho]D0^{+}$, (c) $3^{++}[f_2]P0^{+}$, (e) $3^{++}[\rho_3]S0^{+}$ waves and their corresponding phase differences (b,d,f) with respect to the $2^{-+}[f_2]S0^{+}$ wave. The 27-wave rank-1 fit is shown. Curves show the mass-dependent fits of the $a_3(1874)$ with parameters from Eq. (19). Note that the fitted $a_3(1874)$ mass and width vary considerably in the fits done separately for each decay mode leading to large parameter errors in Eq. (19).

the phase-space factor and the mass-dependent width in the denominator of the Breit-Wigner formula change rapidly in this region.

The ratios of the branching ratios were estimated to be

$$\frac{BR[a_3(1874)\to f_2\pi]}{BR[a_3(1874)\to \rho\pi]}=0.8\pm 0.2,$$
$$\frac{BR[a_3(1874)\to \rho_3\pi]}{BR[a_3(1874)\to \rho\pi]}=0.9\pm 0.3. \tag{20}$$

The observable fractions of 50% $\rho\pi$, 56.5% $f_2\pi$ and 11.8% $\rho_3\pi$ were used in the calculations. Ratios measured by the VES group are 0.45 ± 0.18 and <2.1, respectively (applying the same observable fractions to the results of Ref. [8]). Note that both VES and our results were obtained within the framework of the isobar model. This model may be too restrictive in the case of the $a_3(1874)$ state in view of the predicted large fraction of its genuine 3-body decay [34].

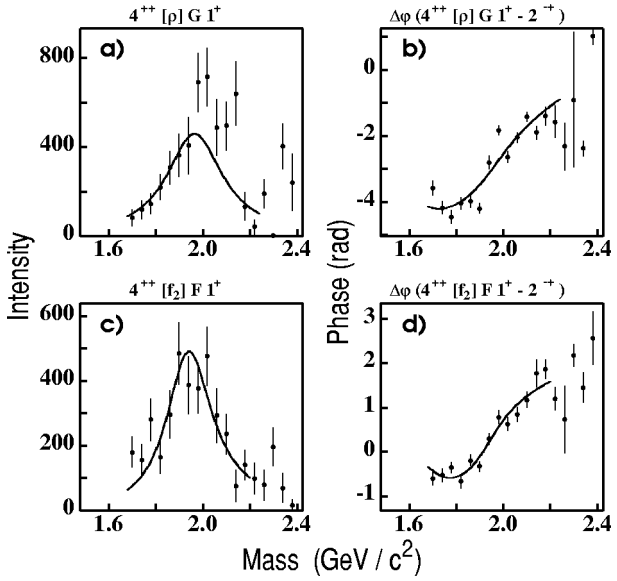

FIG. 17. Intensities of the (a) $4^{++}[\rho]G1^{+}$, (c) $4^{++}[f_2]F1^{+}$ waves and their corresponding phase differences (b,d) with respect to the $2^{-+}[f_2]S0^{+}$ wave. The 27-wave fit is shown. Curves show the mass-dependent fits of the $a_4(2040)$ with parameters from Eq. (21).

$J^{PC}=4^{++}$ waves and $a_4(2040)$

The two strongest 4^{++} waves are $4^{++}[\rho]G1^{+}$ [Fig. 17(a)] and $4^{++}[f_2]F1^{+}$ [Fig. 17(c)] shown in the 27-wave fit. Both waves have a structure in the intensity and a resonant phase motion around 2 GeV/c^2 [Figs. 17(b,d)] and correspond to the known $a_4(2040)$ state. The fitted mass and width of this state are

$$M=1996\pm 25\pm 43 \ \text{MeV}/c^2,$$
$$\Gamma=298\pm 81\pm 85 \ \text{MeV}/c^2, \tag{21}$$

and the decay ratio

$$\frac{BR[a_4(2040)\to \rho\pi]}{BR[a_4(2040)\to f_2\pi]}=1.1\pm 0.2\pm 0.2. \tag{22}$$

The PDG values of the $a_4(2040)$ mass and width are $M=2014\pm 15$ MeV/c^2 and $\Gamma=361\pm 50$ MeV/c^2 [27].

B. The $\pi_1(1600)$ exotic $J^{PC}=1^{-+}$ state

The main result published in our Letter [1] is shown in Fig. 18. The 1^{-+} exotic waves produced in both unnatural (Fig. 18(a)) and natural (Fig. 18(b)) parity exchanges show broad enhancements in the 1.1−1.4 and 1.6−1.7 GeV/c^2 regions. At the same time, the $1^{-+}[f_2]D1^{+}$ wave (not shown) is consistent with zero. The plotted intensities correspond to the 21-wave rank-1 PWA fit. The phase difference between the $1^{-+}[\rho]P1^{+}$ wave and all other significant natural-parity-exchange waves indicates a rapid increase in the phase of the 1^{-+} wave across the 1.5−1.7 GeV/c^2 region; this is consistent with a resonant behavior. Twelve of these phase differences are shown in Fig. 19.

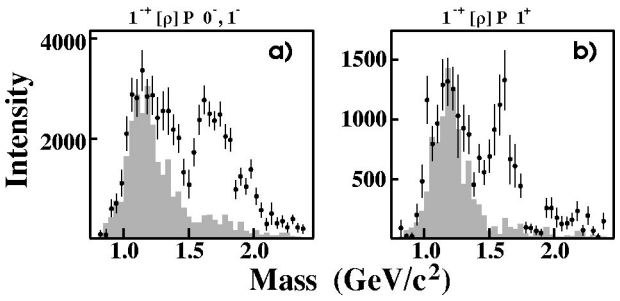

FIG. 18. Wave intensities of the $1^{-+}[\rho]P$ exotic waves: (a) the $M^{\epsilon}=0^-$ and 1^- waves combined; (b) the $M^{\epsilon}=1^+$ wave. The 21-wave rank-1 PWA fit to the data is shown as the points with error bars and the shaded histograms show estimated contributions from all non-exotic waves due to leakage.

(a) Choice of the $\pi\pi$ S-wave parametrization. Extensive studies have been made to test the stability of this result with respect to the assumptions made in the PWA analysis. First, the impact of the particular choice of the $\pi\pi$ *S*-wave isobar parametrization on the 1^{-+} signal was studied. The intensity of the $1^{-+}[\rho]P1^+$ wave and its phase difference with the strongest at the 1.6 GeV/c^2 $2^{-+}[f_2]S0^+$ wave is shown in Fig. 20 for two different PWA fits: with the Au-Morgan-Pennington parametrization of the $\pi\pi$ *S*-wave (our preferred fit), and with the simple Breit-Wigner parametrization of the f_o states. While there are small changes in the shape of the $\pi_1(1600)$ signal (especially at low mass), a similar two-peak structure in the intensity and a similar phase motion are observed in all fits. We conclude that a particular choice of the f_o isobars parametrization does not qualitatively change the resonance behavior of the 1^{-+} wave at 1.6 GeV/c^2.

(b) Study of the t-dependent effects. The implication of fitting the data in a wide interval of the momentum transfer t was also investigated. Strictly speaking, a spin-density matrix should have a limited rank (as assumed in our model) only at a fixed value of t. To study possible consequences of such an assumption, a PWA fit was done in limited intervals of t. As an example, Fig. 21(a) shows the exotic wave intensity for the $0.05<-t<0.15$ $(\mathrm{GeV}/c)^2$ momentum transfer interval. The $\pi_1(1600)$ state is still clearly observed. To further study the t-dependence, the data at 1.6 GeV/c^2 were fitted as a function of t in 0.1 $(\mathrm{GeV}/c)^2$ t-bins. The $M=0$ $1^{++}[\rho]S0^+$ and $2^{-+}[f_2]S0^+$ waves [Figs. 22(a,b)] follow the $e^{-b|t|}$ dependence which is common for the helicity 0 exchange waves. On the other hand, partial waves with non-

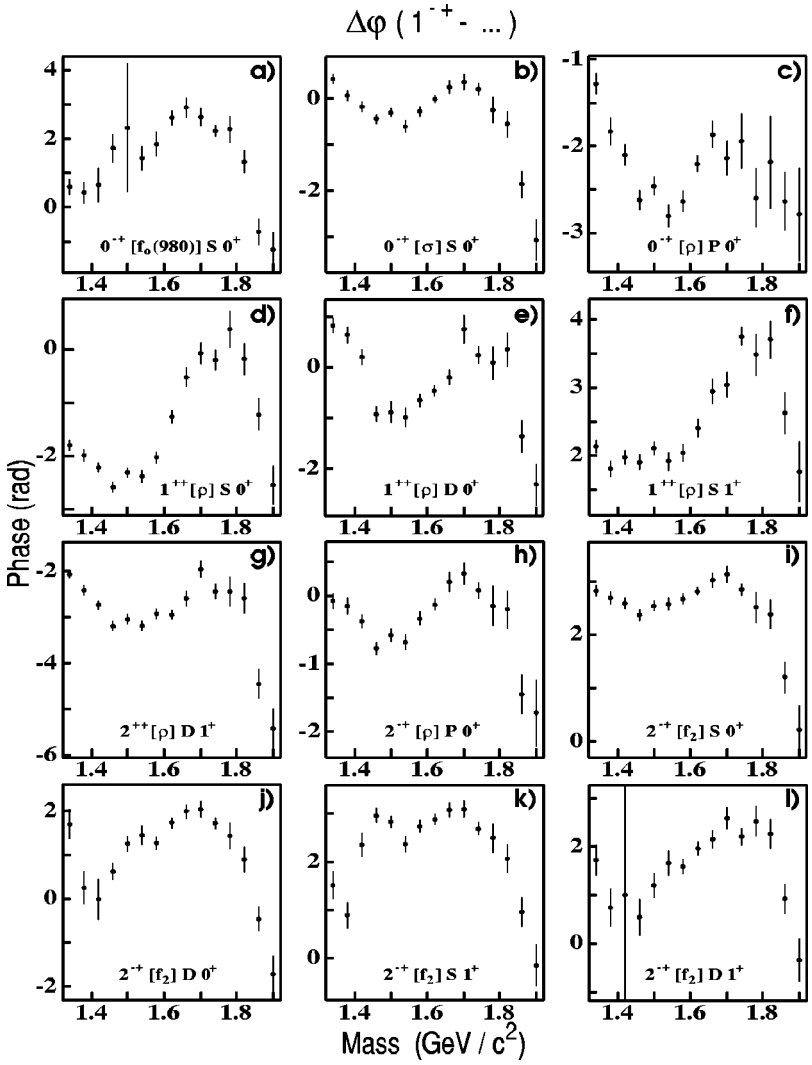

FIG. 19. Phase difference between the $1^{-+}[\rho]P1^+$ wave and (a) the $0^{-+}[f_o(980)]S0^+$ wave; (b) the $0^{-+}[\sigma]S0^+$ wave; (c) the $0^{-+}[\rho]P0^+$ wave; (d) the $1^{++}[\rho]S0^+$ wave; (e) the $1^{++}[\rho]D0^+$ wave; (f) the $1^{++}[\rho]S1^+$ wave; (g) the $2^{++}[\rho]D1^+$ wave; (h) the $2^{-+}[\rho]P0^+$ wave; (i) the $2^{-+}[f_2]S0^+$ wave; (j) the $2^{-+}[f_2]D0^+$ wave; (k) the $2^{-+}[f_2]S1^+$ wave; (l) the $2^{-+}[f_2]D1^+$ wave.

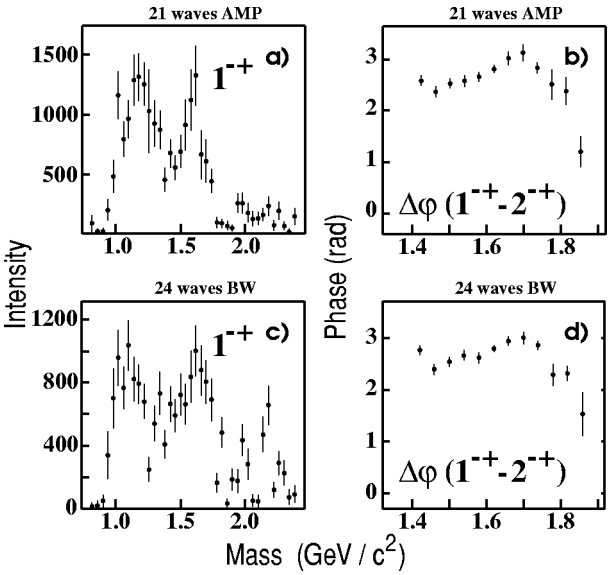

FIG. 20. Intensity of the $1^{-+}[\rho]P1^{+}$ wave (a,c) and its phase difference with respect to the $2^{-+}[f_2]S0^{+}$ wave (b,d) in the 21-wave PWA fit with the Au-Morgan-Pennington parametrization of the $\pi\pi$ *S*-wave (a,b), and the 24-wave PWA fit with the Breit-Wigner parametrization (c,d).

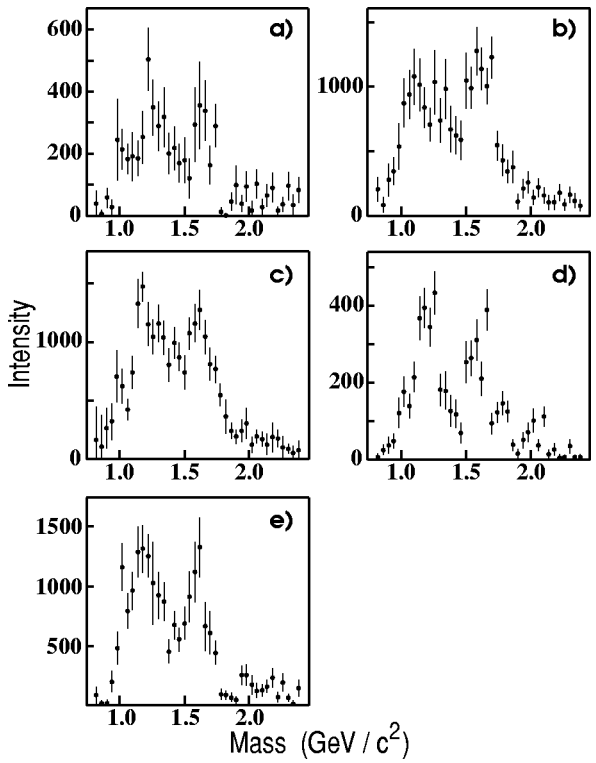

FIG. 21. Intensity of the $1^{-+}[\rho]P1^{+}$ wave in different PWA fits: (a) a fit in the limited range of momentum transfer $0.05<-t<0.15$ $(\mathrm{GeV}/c)^2$; (b) a fit in which events with charged tracks rescattered in the DEA counter were removed; (c) a fit in which events with charged tracks going through the inefficient regions of the drift chambers were removed; (d) a test fit in which an "incorrect" 100% acceptance was assumed. For the purpose of comparison, our preferred 21-wave fit is also shown in (e).

zero helicity exchange are expected to go to 0 at $t=0$ due to angular momentum conservation. Indeed, we find that the $M=1$ projection waves like the $2^{++}[\rho]D1^{+}$ wave [Fig. 22(c)] and, most importantly, the exotic $1^{-+}[\rho]P1^{+}$ wave [Fig. 22(d)] show just such behavior.

(c) Effect of the experimental acceptance. The imperfect knowledge of the experimental acceptance used in a PWA fit is a common source of false signals. We have made a number of tests to check the robustness of the $\pi_1(1600)$ signal to different assumptions used in the Monte Carlo simulation of the apparatus. The majority of such tests are based on exclusion of the events from the regions with a relatively large uncertainty in the instrumental acceptance. Such cuts are applied to both data and Monte Carlo event samples, and a PWA fit is performed. For example, some forward-going tracks may be lost during event reconstruction if they rescatter in the lead-scintillator "sandwich" DEA which is positioned beyond the first 2 drift chamber modules (Fig. 1). Because of a large uncertainty in the Monte Carlo simulation of such events, a requirement of all forward tracks going through the DEA window without rescattering was imposed during event selection. A PWA fit of this event sample is shown in Fig. 21(b). Another potential acceptance problem is a reduced efficiency of the drift chambers at their centers where the high-flux primary beam passes through. This efficiency was parametrized and used at the Monte Carlo stage. To check the validity of such an approach, events with any of the charged tracks going through the inefficient area were eliminated. A PWA fit made with this acceptance cut is shown in Fig. 21(c). The $\pi_1(1600)$ peak in these and many other acceptance tests is clearly visible, and resonance behavior of its phase remains unchanged. Finally, a fit was done in which an incorrect 100% acceptance was assumed. Some partial waves—mostly the 0^{-+} and 2^{-+} waves—undergo a drastic change in this fit. However, the major features of the $1^{-+}[\rho]P1^{+}$ wave were essentially unchanged [Fig. 21(d)].

(d) Effect of the experimental resolution and leakage. While the imperfect knowledge of the experimental acceptance as a source of the spurious $\pi_1(1600)$ signal has been ruled out, the finite instrumental resolution in a situation of a non-uniform acceptance was found to be an important factor in the interpretation of our results. Completely accounting for the finite resolution in the maximum likelihood fit is impractical. Instead, the following study has been done.

Four sets of Monte Carlo events were generated and distributed as the $1^{++}[\rho]S0^{+}$, $2^{++}[\rho]D1^{+}$, $2^{-+}[f_2]S0^{+}$ or $2^{-+}[\rho]P0^{+}$ waves—the four largest waves in this reaction. The generated "pure wave" event samples were used in the maximum likelihood fit instead of the real data. This allows the study of possible leakage from the major waves into other waves which were not present in the generated samples. At first, a 100% acceptance was assumed to study leakage due to statistical fluctuations only. Such leakage was found to be negligible in any of the partial waves.

The generated events were put through a program of Monte Carlo simulation of the apparatus to study the effects of the finite resolution and limited acceptance, and the partial wave fit was redone. Leakage into the 1^{-+} waves from the

$2^{++}[\rho]D1^+$, $2^{-+}[f_2]S0^+$ and $2^{-+}[\rho]P0^+$ waves was still negligible and consistent with the statistical fluctuations. However, leakage from the $1^{++}[\rho]S0^+$ wave into the 1^{-+} waves changed drastically. Above 1.5 GeV/c^2 the fitted intensity of leakage into the 1^{-+} waves was less than 1% of the initially generated 1^{++} intensity and consistent with statistical fluctuations. Below this, mass leakage was noticeable: 5–6 % at 1.3 GeV/c^2 growing to 10–15 % at 1.0 GeV/c^2. Some other waves such as the $2^{-+}[\rho]P0^+$ wave were also contaminated by leakage.

Qualitatively, such leakage can be explained by the shape of the experimental acceptance in the Gottfried-Jackson frame [Fig. 5(c)] and by the mass dependence of the acceptance [Fig. 5(a)]. The initially flat $\rho\pi$ S wave would have a shape of Fig. 5(c) when the experimental acceptance is applied. The finite resolution smears this distribution leading to an apparent excess of observed events at $\cos\theta_{GJ}=\pm 1$. Such an excess of events will be accommodated by a PWA fit through the combination of initially non-existent waves, mostly the $\rho\pi$ P waves. A drop in the acceptance at low 3π masses makes the problem worse there, leading to an increased leakage at small mass.

To estimate the actual level of leakage in the 1^{-+} signal, Monte Carlo events were generated in accordance with the spin-density matrix $\rho^{\epsilon}_{\alpha\alpha'}$ found in the 21-wave fit of the real data, except for the matrix elements corresponding to the 1^{-+} waves which were set to zero. This is done by calculating a weight factor

$$w_i=\sum_{\epsilon}\sum_{\alpha,\alpha'}\Psi^{\epsilon}_{\alpha}(\tau_i)\rho^{\epsilon}_{\alpha\alpha'}\Psi^{\epsilon}_{\alpha'}{}^{*}(\tau_i) \tag{23}$$

for each phase-space Monte Carlo event with a subsequent random selection of the events based on their weight. Here $\Psi^{\epsilon}_{\alpha}(\tau_i)$ is the decay amplitude of the wave α calculated at the phase-space point τ_i of the i-th event. The Monte Carlo simulation of the instrumental acceptance and resolution was applied to the generated events. Intensities of the 1^{-+} waves found in the partial-wave fit of this sample are shown as shaded histograms in Fig. 18. Considerable leakage from the non-exotic waves to the 1^{-+} waves is evident below 1.4 GeV/c^2. The presence of leakage prevents us from drawing any conclusion about the nature of the low-mass enhancement in the 1^{-+} spectrum. However, the second peak in the 1^{-+} intensities at 1.6 GeV/c^2 (where resonant behavior is observed) is essentially not affected by the leakage problem.

(e) Choice of the rank of the fit and the set of partial waves. We have also studied how our results for the exotic 1^{-+} wave are affected by the restriction on the rank of the spin-density matrix and by the choice of the partial waves used in the PWA fit. A comparison of the rank 1 and rank 2 fits for the same 21 waves as well as a comparison of the 21-wave and 27-wave fits for the same rank is illustrated in Fig. 23. We have found that there is a clear variation in the shape and magnitude of the $\pi_1(1600)$ signal produced in the natural parity exchange [Figs. 23(a,c)]. The $\pi_1(1600)$ peak appears to be somewhat broader in PWA fits with many more

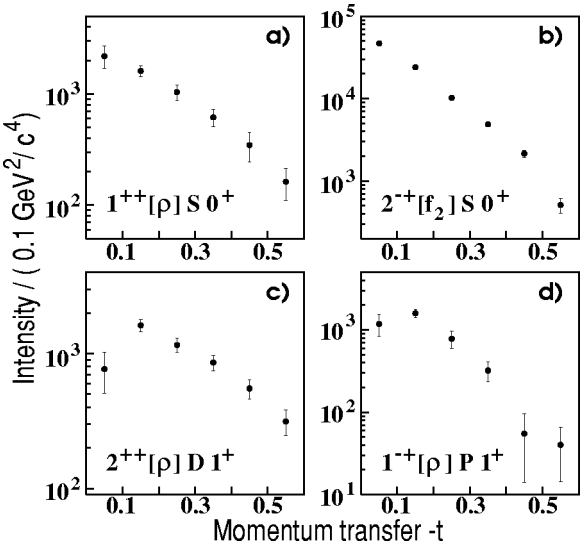

FIG. 22. Intensity of some partial waves at 1.6 GeV/c^2 as a function of the momentum transfer $-t$: (a) The $1^{++}[\rho]S0^+$ wave; (b) the $2^{-+}[f_2]S0^+$ wave; (c) the $2^{++}[\rho]D1^+$ wave; (d) the $1^{-+}[\rho]P1^+$ wave.

fitted parameters. However, a structure at 1.6 GeV/c^2 in the $M^{\epsilon}=1^+$ wave is always present, and its phase always exhibits a resonance behavior [as seen in Figs. 23(b,d), the resonant phase motion of the well-established $\pi_2(1670)$ is always compensated by the resonant phase motion of the $\pi_1(1600)$ leading to an almost flat phase difference between them] albeit a less stable one in the fits with many more fitted parameters. These variations lead to the rather large model-dependent systematic uncertainties which we assign

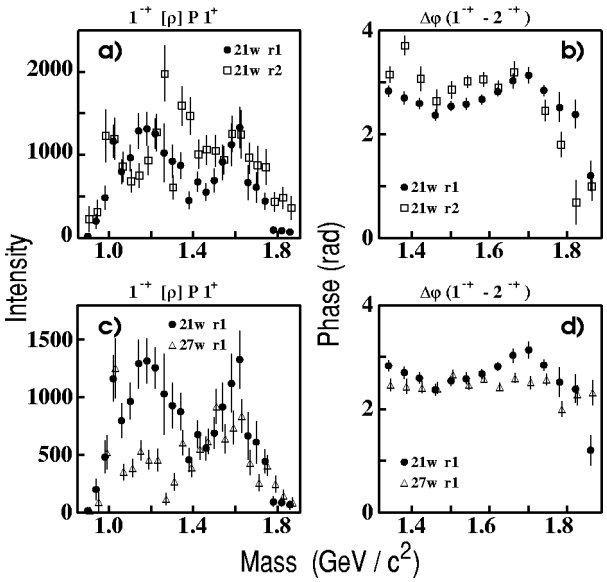

FIG. 23. Intensity of the $1^{-+}[\rho]P1^+$ wave (a,c) and its phase difference with respect to the $2^{-+}[f_2]S0^+$ wave (b,d) in 3 different PWA fits: 21-wave rank-1 (closed circles), 21-wave rank-2 (open squares), and 27-wave rank-1 (open triangles). Rank-1 and rank-2 fits are compared in the top row while 21-wave and 27-wave fits are shown in the bottom row.

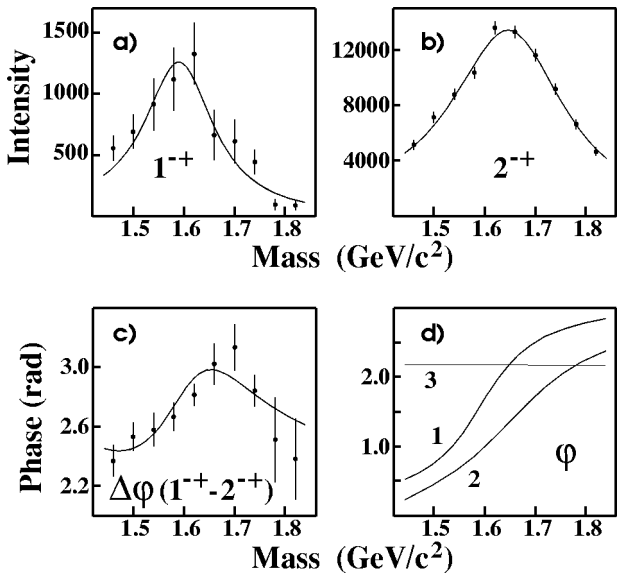

FIG. 24. A coupled mass-dependent Breit-Wigner fit of the $1^{-+}[\rho(770)]P1^{+}$ and $2^{-+}[f_2(1270)]S0^{+}$ waves. (a) $1^{-+}[\rho(770)]P1^{+}$ wave intensity. (b) $2^{-+}[f_2(1270)]S0^{+}$ wave intensity. (c) Phase difference between the $1^{-+}[\rho(770)]P1^{+}$ and $2^{-+}[f_2(1270)]S0^{+}$ waves. (d) Phase motion of the $1^{-+}[\rho(770)]P1^{+}$ wave (1), $2^{-+}[f_2(1270)]S0^{+}$ wave (2), and the production phase between them (3).

to the parameters of the 1^{-+} state. In the unnatural parity sector, the $M^{\epsilon}=1^{-}$ wave exhibits very strong model dependence, almost disappearing in the fits with larger numbers of partial waves. The $M^{\epsilon}=0^{-}$ wave is more stable but it peaks above 1.7 GeV/c^2—significantly higher than the $\pi_1(1600)$ state in the natural parity exchange. We note that Ref. [8], which is based on the 3π data obtained at about twice as high beam energy than in our experiment, claims to see no significant intensity in the unnatural parity sector. This can be understood in terms of Regge phenomenology in which cross sections for unnatural parity exchanges (for example, b_1 or f_1 exchanges) are expected to fall rapidly with energy. We find that a combined contribution of all unnatural parity waves already at 18 GeV/c is no more than 1–5 % of the total intensity. As a result, there are no significant waves in the unnatural parity exchange sector with which to conduct phase studies of the 1^{-+} signal. Without such a study, the nature of the 1^{-+} waves in the unnatural parity exchange sector remains unclear.

The phase study is possible in the natural parity exchange sector. To conduct such a study and to determine the resonance parameters of the 1^{-+} state, a series of two-state χ^2 fits of the $1^{-+}[\rho]P1^{+}$ and $2^{-+}[f_2]S0^{+}$ waves as a function of mass was made. The latter wave was chosen as an anchor because it is a major decay mode of the $\pi_2(1670)$, the only well-established resonance in the vicinity of 1.6 GeV/c^2. An example of such fits is shown in Fig. 24. This plot corresponds to the 21-wave rank-1 PWA fit. The χ^2 function of the fit is $\chi^2=\Sigma Y_i^T E_i^{-1} Y_i$, where Y_i is a 3-element vector consisting of the differences between measured and parametrized values for the intensities of both waves and the phase difference between them in the mass bin i, and E_i is a 3×3 error matrix for these values calculated through Jacobian transformation from the error matrix of production amplitudes found in the maximum likelihood fit. Both waves are parametrized with relativistic Breit-Wigner forms including Blatt-Weisskopf barrier factors. In addition to Breit-Wigner phases, a production phase difference which varies linearly with mass is assumed. The fit shown in Fig. 24 yields $\chi^2=25.8$ for 22 degrees of freedom, with the production phase difference between the two waves being almost constant throughout the region of the fit. The mass and width of the $\pi_1(1600)$ state found in this fit are 1593 MeV/c^2 and 168 MeV/c^2 correspondingly. If instead the 1^{-+} wave is assumed to be non-resonant (with no phase motion), then the fit has $\chi^2=50.8$ for 22 degrees of freedom, and requires a production phase with a slope of 7.6 radians/(GeV/c^2). Such rapid variation of the production phase makes a non-resonant interpretation of the 1^{-+} wave unlikely. Attempts to use a constant production phase in a non-resonant case result in a totally unacceptable fit with χ^2/degree of freedom$=396.6/23$.

We choose this PWA fit (21-wave rank 1) as the basis for quoting the $\pi_1(1600)$ mass and width because it gives a satisfactory description of all observables (moments, angular distributions, Dalitz plots, etc.) using the minimal number of free parameters among all acceptable PWA fits. The systematic errors on the $\pi_1(1600)$ resonance parameters were estimated by fitting the PWA results obtained for different sets of partial waves and different rank of the PWA fit. Different $\pi_2(1670)$ and $\pi(1800)$ waves were used as anchor waves in these fits. In some of them, the $\pi_1(1600)$ was found to be much broader than in our preferred fit resulting in an unusually large upper systematic error which we assign to the $\pi_1(1600)$ width. The fitted mass and width of the 1^{-+} state are

$$M=1593\pm8^{+29}_{-47}\ \text{MeV}/c^2,$$
$$\Gamma=168\pm20^{+150}_{-12}\ \text{MeV}/c^2. \tag{24}$$

The error values correspond to statistical and systematic uncertainties, respectively.

Our recent analysis of the $\eta'\pi^-$ state [7] confirmed the existence of the $\pi_1(1600)$ exotic meson. In this channel, the following $\pi_1(1600)$ parameters were obtained: $M=1597\pm10^{+45}_{-10}$ MeV/c^2, $\Gamma=340\pm40\pm50$ MeV/c^2. A combined fit of the PWA results for the $\eta'\pi^-$, $\rho\pi$ and $b_1(1235)\pi$ channels was done by the VES group for their data [8]. They conclude that a broad 1^{-+} state is seen in all three decays with comparable branching ratios. They quote the following $\pi_1(1600)$ parameters: $M=1560\pm60$ MeV/c^2, $\Gamma=340\pm50$ MeV/c^2. Large error bars allow these measurements to be consistent with each other. A search for the $\pi_1(1600)$ exotic meson in other channels is necessary to determine its width with a better precision.

V. SUMMARY AND CONCLUSIONS

The main results of this paper are summarized in Table II and below.

TABLE II. Summary of the numerical results presented in this paper.

Resonance parameters

J^{PC} Resonance and decay mode(s) used	M, MeV/c^2	Γ, MeV/c^2
$0^{-+}\pi(1300)\to\rho(770)\pi$	$1343\pm15\pm24$	$449\pm39\pm47$
$0^{-+}\pi(1800)\to f_o(980)\pi$	$1774\pm18\pm20$	$223\pm48\pm50$
$0^{-+}\pi(1800)\to\sigma\pi$	$1863\pm9\pm10$	$191\pm21\pm20$
$1^{-+}\pi_1(1600)\to\rho(770)\pi$	$1593\pm8^{+29}_{-47}$	$168\pm20^{+150}_{-12}$
$1^{++}a_1(1700)\to\rho(770)\pi$	$1714\pm9\pm36$	$308\pm37\pm62$
$2^{-+}\pi_2(1670)\to f_2(1270)\pi$	$1676\pm3\pm8$	$254\pm3\pm31$
$2^{++}a_2(1320)\to\rho(770)\pi$	$1326\pm2\pm2$	$108\pm3\pm15$
$3^{++}a_3(1874)\to\rho(770)\pi, f_2(1270)\pi, \rho_3(1690)\pi$	$1874\pm43\pm96$	$385\pm121\pm114$
$4^{++}a_4(2040)\to\rho(770)\pi, f_2(1270)\pi$	$1996\pm25\pm43$	$298\pm81\pm85$

Ratio of branching ratios

Numerator	Denominator	Ratio
$\pi(1800)\to f_o(980)\pi, f_o(980)\to\pi\pi$	$\pi(1800)\to\sigma\pi, \sigma\to\pi\pi$	$0.44\pm0.08\pm0.38$
$\pi_2(1670)\to f_2(1270)\pi, f_2\to\pi\pi$	$\pi_2(1670)\to\sigma\pi, \sigma\to\pi\pi$	$4.9\pm0.6\pm2.0$
$\pi_2(1670)\to f_2(1270)\pi$	$\pi_2(1670)\to\rho(770)\pi$	$2.33\pm0.21\pm0.31$
$a_3(1874)\to f_2(1270)\pi$	$a_3(1874)\to\rho(770)\pi$	0.8 ± 0.2
$a_3(1874)\to\rho_3(1690)\pi$	$a_3(1874)\to\rho(770)\pi$	0.9 ± 0.3
$a_4(2040)\to\rho(770)\pi$	$a_4(2040)\to f_2(1270)\pi$	$1.1\pm0.2\pm0.2$

Ratio of wave amplitudes

Resonance and decay mode	Waves	Ratio
$D/S[a_1(1260)\to\rho(770)\pi]$	$1^{++}[\rho]D0^+/1^{++}[\rho]S0^+$	$-0.14\pm0.04\pm0.07$[a]
$F/P[\pi_2(1670)\to\rho(770)\pi]$	$2^{-+}[\rho]F0^+/2^{-+}[\rho]P0^+$	$-0.72\pm0.07\pm0.14$

[a]Deck-type background was not subtracted.

(i) A partial-wave analysis of the reaction $\pi^- p\to\pi^+\pi^-\pi^- p$ has been performed on a data sample of 250 000 events.

(ii) The well-known states $a_1(1260)$, $a_2(1320)$, $\pi_2(1670)$ are observed. The $\pi_2(1670)$ branching ratios are measured for the decay channels available in this reaction.

(iii) The 0^{-+} $\pi(1300)$ resonance is seen in the $\rho\pi$ and, possibly, $\sigma\pi$ channels.

(iv) The 0^{-+} $\pi(1800)$ state is found in the $f_o(980)\pi$ and $\sigma\pi$ channels. There is an indication of two possible 0^{-+} states at 1.8 GeV/c^2.

(v) The 1^{++} $a_1(1700)$ meson is seen in the $\rho\pi$ D wave.

(vi) The ratio of the D and S wave amplitudes for the $a_1(1260)\to\rho\pi$ decay (ignoring the Deck-effect contribution) is found to be in agreement with the ^3P_o model prediction.

(vii) The 3^{++} a_3 state is found in the $\rho\pi$, $f_2\pi$ and $\rho_3\pi$ channels.

(viii) The 4^{++} $a_4(2040)$ resonance is observed in the $\rho\pi$ and $f_2\pi$ channels.

(ix) The exotic $J^{PC}=1^{-+}$ $\rho\pi$ wave produced by natural parity exchange has structure in the intensity and phase motion consistent with the presence of the $\pi_1(1600)$ resonance. This state has a resonance mass of $1593\pm8^{+29}_{-47}$ MeV/c^2 and a width of $168\pm20^{+150}_{-12}$ MeV/c^2.

(x) A strong PWA model dependence of the shape and magnitude of the $\pi_1(1600)$ signal is observed.

ACKNOWLEDGMENTS

The authors wish to acknowledge the invaluable help of the staff at the MPS facility in carrying out this experiment and the assistance of the staffs of the AGS, BNL, and the collaborating institutions. This research was supported in part by the U.S. Department of Energy, the National Science Foundation, and the Russian Ministry of Science and Technology.

[1] E852 Collaboration, G.S. Adams *et al.*, Phys. Rev. Lett. **81**, 5760 (1998).

[2] S. Godfrey and N. Isgur, Phys. Rev. D **32**, 189 (1995).

[3] KEK-179 Collaboration, H. Aoyagi *et al.*, Phys. Lett. B **314**, 246 (1993).

[4] VES Collaboration, G.M. Beladidze *et al.*, Phys. Lett. B **313**, 276 (1993).

[5] E852 Collaboration, D.R. Thompson *et al.*, Phys. Rev. Lett. **79**, 1630 (1997).

[6] Crystal Barrel Collaboration, W. Dünnweber *et al.*, in *Pro-*

ceedings of the VII International Conference on Hadron Spectroscopy, edited by S.U. Chung and H.J. Willutzki, AIP Conf. Proc. No. 432 (AIP, New York, 1998), p. 309; A. Abele *et al.*, Phys. Lett. B **423**, 175 (1998).
[7] E852 Collaboration, E.I. Ivanov *et al.*, Phys. Rev. Lett. **86**, 3977 (2001).
[8] VES Collaboration, A. Zaitsev, Nucl. Phys. **A675**, 155c (2000).
[9] VES Collaboration, Yu.P. Gouz *et al.*, in *Proceedings of the XXVI International Conference on High Energy Physics*, edited by J.R. Sanford, AIP Conf. Proc. No. 272 (AIP, New York, 1993), Vol. 1, p. 572.
[10] E818 Collaboration, J.H. Lee *et al.*, Phys. Lett. B **323**, 227 (1994).
[11] N. Isgur and J. Paton, Phys. Rev. D **31**, 2910 (1985).
[12] C. Bernard *et al.*, Phys. Rev. D **56**, 7039 (1997); P. Lacock *et al.*, Phys. Lett. B **401**, 308 (1997).
[13] T. Barnes and F.E. Close, Phys. Lett. **116B**, 365 (1982).
[14] I.I. Balitsky, D.I. Dyakonov, and A.V. Yung, Z. Phys. C **33**, 265 (1986); J.I. Latorre, P. Pascual, and S. Narison, *ibid.* **34**, 347 (1987); J. Govaerts *et al.*, Nucl. Phys. **B284**, 674 (1987); S. Narison, Nucl. Phys. **A675**, 54c (2000).
[15] Y. Uehara *et al.*, Nucl. Phys. **A606**, 357 (1996).
[16] S. Ishida *et al.*, Phys. Rev. D **47**, 179 (1993).
[17] T. Barnes, F.E. Close, and E.S. Swanson, Phys. Rev. D **52**, 5242 (1995).
[18] F.E. Close and P.R. Page, Nucl. Phys. **B443**, 233 (1995).
[19] E852 Collaboration, Z. Bar-Yam *et al.*, Nucl. Instrum. Methods Phys. Res. A **386**, 253 (1997).
[20] E852 Collaboration, T. Adams *et al.*, Nucl. Instrum. Methods Phys. Res. A **368**, 617 (1996).
[21] S.E. Eiseman *et al.*, Nucl. Instrum. Methods Phys. Res. A **217**, 140 (1983).
[22] E852 Collaboration, R.R. Crittenden *et al.*, Nucl. Instrum. Methods Phys. Res. A **387**, 377 (1997).
[23] E852 Collaboration, S. Teige *et al.*, Phys. Rev. D **59**, 012001 (1999).
[24] O.I. Dahl *et al.*, ''SQUAW kinematic fitting program,'' Group A programming note P-126, Univ. of California, Berkley (1968).
[25] S.U. Chung, ''Formulas for Partial-Wave Analysis,'' Report BNL-QGS-93-05, Brookhaven National Laboratory (1993); J.P. Cummings and D.P. Weygand, ''The New BNL Partial Wave Analysis Programs,'' Report BNL-64637, Brookhaven National Laboratory (1997).
[26] S.U. Chung and T.L. Trueman, Phys. Rev. D **11**, 633 (1975).
[27] Particle Data Group, L. Montanet *et al.*, Phys. Rev. D **50**, 1173 (1994); D.E. Groom *et al.*, Eur. Phys. J. C **15**, 1 (2000).
[28] Crystal Barrel Collaboration, C. Amsler *et al.*, Phys. Lett. B **342**, 443 (1995).
[29] S.U. Chung *et al.*, Ann. Phys. (Leipzig) **4**, 404 (1995).
[30] I.J.R. Aitchison, Nucl. Phys. **A189**, 417 (1972).
[31] K.L. Au, D. Morgan, and M.R. Pennington, Phys. Rev. D **35**, 1633 (1987).
[32] VES Collaboration, D.V. Amelin *et al.*, Phys. Lett. B **356**, 595 (1995).
[33] E852 Collaboration, S.U. Chung *et al.*, Phys. Rev. D **60**, 092001 (1999).
[34] T. Barnes *et al.*, Phys. Rev. D **55**, 4157 (1997).
[35] SERPUKHOV-080 Collaboration, G. Bellini *et al.*, Phys. Rev. Lett. **48**, 1697 (1981).
[36] F.E. Close and P.R. Page, Phys. Rev. D **56**, 1584 (1997).
[37] Crystal Barrel Collaboration, U. Thoma, Nucl. Phys. **A675**, 76c (2000).
[38] G. Ascoli *et al.*, Phys. Rev. D **8**, 3894 (1973).